

# Prediction of Yield Strength from Chemistry and Grain Size Using Historical Models

Peter Martin<sup>1</sup>, Nathan Switzner<sup>1</sup>, Owen Lopez-Oneal<sup>2</sup>, Sophia Curiel<sup>2</sup>,  
Peter Veloo<sup>2</sup>

<sup>1</sup>RSI Pipeline Solutions <sup>2</sup>Pacific Gas and Electric



Organized by



*Proceedings of the 2025 Pipeline Pigging and Integrity Management Conference.*

Copyright © 2025 by Clarion Technical Conferences and the author(s).

*All rights reserved. This document may not be reproduced in any form without permission from the copyright owners.*

## Abstract

It is widely accepted that the yield strength of low carbon and low alloy steels can be modeled as the sum of contributions from intrinsic lattice friction stress and a few known strengthening mechanisms. These mechanisms, which include solid solution strengthening, grain size effects, dispersion strengthening, and dislocation density, have been extensively reported upon in published research dating back as far as the 1930s. Simple, representative models have been shown to be accurate and effective, but line pipe applications have been limited because the quantitative metallography required to determine grain size has historically been time consuming and resource intensive. The recent development of a machine learning model to perform rapid, reliable grain size measurements warrants revisiting these models.

The yield strengths for a set of 38 hot-rolled, non-microalloyed steels were estimated from the %Mn, %Si, %Cr, %Cu, and grain size using the model published by Pickering in 1978. Grain size and solid solution contributions were calculated using only the original coefficients published in 1978, while the contribution of dislocation density was estimated by assuming a constant, average dislocation density for all the pipes. Comparison of model predictions to yield strengths from tensile testing resulted in a mean absolute percent error (MAPE) of 8.0% with a 95% prediction interval of  $\pm 11.8$  ksi. This performance compares favorably to the instrumented indentation test (IIT), where comparison to tensile testing for an expanded set of 83 pipes yields a mean absolute percent error (MAPE) of 8.6% with a 95% prediction interval of  $\pm 12.2$  ksi. The results suggest that this model may be a useful tool to confirm strength testing by IIT, provide strength estimates where IIT is not practical, or replace some fraction of strength testing altogether.

## Introduction

This investigation illustrates the use of an historical strength model for steel to estimate yield strength from grain size and composition in line pipe steels. The use of this type of simple, representative model for line pipe applications has been limited because the quantitative metallography required to determine grain size has historically been time consuming and resource intensive [1,2]. The recent development of a machine learning model to perform rapid, reliable grain size measurements decreases those concerns and warrants revisiting these models [3]. Although, microstructural analysis already provides insights about line pipe vintage and manufacturing processes [4], the ability to estimate yield strength using microstructural and compositional analysis would provide additional value. Past research has shown the merit of microstructural considerations being used to improve non-destructive estimation of yield strength [5], but the present work is focused on utilizing microstructure and composition to predict yield strength independent of other non-destructive strength test data.

According to several established models [6,7,8], the yield strength,  $\sigma_y$ , of ferritic steels can be factorized into a number of intrinsic components:

$$\sigma_Y = \sigma_0 + \sigma_{SS} + \sigma_{GS} + \sigma_{dis} + \sigma_{ppt} \tag{1}$$

where  $\sigma_0$  is the intrinsic lattice friction stress, and  $\sigma_{SS}$ ,  $\sigma_{GS}$ ,  $\sigma_{dis}$ , and  $\sigma_{ppt}$  are contributions from solid solution, grain size, dislocation, and precipitation strengthening, respectively. The solid solution strengthening can be estimated from the Pickering strength model [9]:

$$\sigma_{SS} = \sum(C_i \cdot \%A_i) \tag{2}$$

[MPa, weight %]

where  $C_i$  are coefficients and  $A_i$  represent the weight percent of the  $i = 1$  to  $n$  primary alloying constituents (e.g., Mn, Si, etc.). Grain size strengthening can be expressed from the well-known Hall-Petch equation [8,10,11,12]:

$$\sigma_{GS} = k \cdot d^{-0.5} \tag{3}$$

[MPa, mm]

where  $k$  is a constant and  $d$  is the average grain size of ferrite (in mm) determined by the linear intercept method. The strengthening contribution due to dislocations can be calculated using the Taylor relation [8,13-15]:

$$\sigma_{dis} = M \cdot \alpha \cdot G \cdot b \cdot \rho^{0.5} \tag{4}$$

[MPa, MPa, m, m<sup>-2</sup>]

where  $M$  and  $\alpha$  are constants,  $G$  is the shear modulus of the ferrite,  $b$  is the Burgers vector of the dislocations, and  $\rho$  is the dislocation density. Finally, the degree of strengthening due to nano-sized precipitates is dependent on both their fraction and size in the microstructure per the Ashby-Orowan model [16]; however, a simplified empirical relation can be used to describe this effect for relevant precipitate species such as V<sub>4</sub>C<sub>3</sub>, VN, Nb(CN) and TiC [8]:

$$\sigma_{ppt} = B \cdot (\%solute) \tag{5}$$

[MPa, weight %]

For the pipe samples used in the current investigation, the concentrations of V, Nb and Ti were low and the measurement results for those elements were low-resolution. As a result, no useful correlation was observed between the yield strength measured by tensile testing ( $\sigma_{TT}$ ) and the precipitation-hardening term ( $\sigma_{ppt}$ ); therefore, that term was excluded from the subsequent analysis.

Combining Eqs. 1 - 4 yields:

$$\sigma_Y = \sigma_0 + \sum(C_i \cdot \%A_i) + k \cdot d^{-0.5} + M \cdot \alpha \cdot G \cdot b \cdot \rho^{0.5} \tag{6}$$

**Table 1:** Published values of the parameters from Eq. (6) [9].

Parameter	Value	Units
$\sigma_0$	53.9	MPa
$k$	17.4	MPa·√mm
$M\alpha$	0.38	-
$G$	81.6x10 <sup>3</sup>	MPa
$b$	0.249	nm
$C_{Si}$	85	MPa
$C_{Cu}$	38	MPa
$C_{Mn}$	32	MPa
$C_{Cr}$	-30	MPa

Theoretical values are available in the literature for the terms  $\sigma_0$ ,  $G$ , and  $b$ , as well as empirical or semi-empirical values for the coefficients  $C_i$ ,  $k$ , and  $M\alpha$  (Table 1) [9]. The alloying compositions  $\%A_i$  can be obtained by nondestructive testing (NDT) or destructive measurements (DT), and the average grain size  $d$  can be determined from analysis of microstructures obtained from nondestructive surface replicas or destructive cross-sections. In most cases, there is no practical field measurement for the dislocation density. In the present investigation, a

representative average value for the contribution from dislocation density was estimated from the average difference between  $\sigma_{TT}$  and the sum of the remaining terms from Eq. 6. This approach was justified by the similarity in the pipe microstructures, which are all comprised of ferrite-pearlite associated with hot- or controlled-rolling without the transformation products associated with quenching and tempering.

The historical model provides a few novel differences from machine learning or neural network based approaches developed more recently [17]. The formulation of the model provides a clear accounting of the contributing mechanisms using established models and coefficients. The historical nature of the model suggests broad applicability and reliable performance that has been validated over several decades, and it minimizes the reliance upon ‘calibration’ against a known, relevant set of pipes, a.k.a., training data. Improved performance can be achieved by the use of fitted rather than published, historical coefficients. While this decreases the scatter and prediction intervals, it introduces some risk of limiting the applicability of the model to populations for which the pipe data used to generate the coefficients are representative. For now, the recommended approach is to maximize the applicability of the model by using the literature values from Table 1 for the coefficients while applying an estimated average dislocation density determined by fitting Eq. 6 to  $\sigma_{TT}$  for the current set of known pipes.

## Materials and Methods

### Pipe Samples

The materials used in this work comprised 38 pipes with available results from tensile testing, destructive (laboratory) chemistry analysis, nondestructive (field) chemistry analysis, destructive cross-section metallography, and nondestructive replica metallography. The samples included examples of seamless (SMLS), submerged arc welded (SAW), electric resistance welded (ERW), and flash welded line pipe. Manufacturing dates ranged from 1931 to 2017, grade ranged from B to X70, and OD ranged from 0.215 in. to 0.500 in. The characteristics of the individual pipes are summarized in Table 2. Note that quenched and tempered pipe, as well as fabricated components like elbows, reducers, tees, and caps, were excluded from the analyses due to the unknown potential impact of the different thermomechanical process routes.

### Test Methods

Benchmark destructive testing (DT) values for yield strength ( $\sigma_{TT}$ ) at 0.5% elongation under load (EUL) were obtained from uniaxial tension tests performed on full wall thickness ‘straps’ removed from each pipe. The straps were oriented in the transverse direction and were flattened in a press prior to testing. Nominal strap dimensions conformed to API 5L and ASTM A370, including gage length of 2.0 in. (51 mm), width of 1.5 in. (38 mm), and thickness equal to the full pipe wall thickness. Testing was performed in displacement control at a rate of 0.05 in./min ( $3 \times 10^{-2}$  mm/s), and the reported values represent the average of four tests.

Yield strengths were also obtained nondestructively (NDT) by instrumented indentation testing ( $\sigma_{IT}$ ) using a Frontics AIS 2100 system equipped with a 500  $\mu\text{m}$  diameter spherical indenter. The test sequence applied 15 displacement-controlled load-unload cycles, with the indentation depth increasing by 10  $\mu\text{m}$  for each cycle to reach a final depth of 150  $\mu\text{m}$ . The load-depth data were subsequently post-processed in R to convert the maximum load and the corresponding indenter depth for each cycle into representative stresses using the algorithm described in [18,19].

DT chemistry values were obtained by spark optical emission spectroscopy (SOES) for Cr, Cu, Mn, and Si in accordance with ASTM E415. NDT chemistry values were obtained by atomic absorption performed on filings (burrs) removed from the pipe surfaces by the processes detailed in references [20,21,22].

For microstructure, standard (destructive / DT) cross-sections were prepared from cut-outs from the pipes [23]. The cut-outs were mounted, ground, polished with a final polishing step of 1  $\mu\text{m}$  diamond polishing paste, and etched with 5% nital (5% nitric acid in methanol) for 5-30 seconds to reveal the microstructure. Additionally, nondestructive (NDT) replicas of the pipe surfaces were prepared using methods consistent with nondestructive field metallography [23]. After removal of 0.010 in. ( $\approx 260 \mu\text{m}$ ) from the pipe surface, a 1 in. by 1 in. (25 mm by 25 mm) square area was manually ground, polished to a finish of 1  $\mu\text{m}$ , and etched with 5% nital. Surface replicas were prepared using acetate tape wetted with acetone.

**Table 2.** Characteristics of the 38 pipes used in the present investigation. In the last column,  $\sigma_{IT}$  represents the 0.5% elongation under load yield strength determined from tensile testing.

No.	Seam	Grade	Year	OD, in.	WT, in.	$\sigma_{IT}$ , ksi
1	SAW	Unk.	Unk.	14.0	0.253	45.1
2	SAW	Unk.	Unk.	24.0	0.281	73.5
3	SAW	Unk.	Unk.	24.0	0.281	71.1
4	SAW	Unk.	Unk.	24.0	0.281	74.2
5	SAW	Unk.	Unk.	24.0	0.281	73.1
6	SAW	X52	1979	24.0	0.265	61.0
7	SAW	X65	2017	30.0	0.500	73.2
8	SAW	Unk.	Unk.	36.0	0.349	68.9
9	SAW	X65	2014	36.0	0.500	70.6
10	SAW	X52	2014	36.0	0.500	55.6
11	ERW	B	1952	8.625	0.250	52.1
12	ERW	B	1954	10.75	0.313	49.1
13	ERW	B	2007	16.0	0.313	67.1
14	ERW	X52	1957	16.0	0.386	55.3
15	ERW	X52	1957	16.0	0.261	56.5
16	ERW	Unk.	Unk.	18.0	0.261	53.2
17	ERW	X70	2016	20.0	0.500	75.4
18	ERW	X65	2017	24.0	0.500	79.2
19	ERW	X52	2017	24.0	0.500	63.8
20	ERW	X52	Unk.	24.0	0.267	57.0
21	Flash	Unk.	Unk.	16.0	0.267	58.2
22	Flash	Unk.	Unk.	16.0	0.256	53.8
23	Flash	Unk.	Unk.	26.0	0.289	59.9
24	SMLS	B	1931	8.625	0.215	48.3
25	SMLS	B	1952	8.625	0.250	44.6
26	SMLS	B	1952	8.625	0.250	48.0
27	SMLS	B	1986	8.625	0.322	59.7
28	SMLS	B	1947	8.625	0.277	48.9
29	SMLS	B	1949	12.75	0.313	49.3
30	SMLS	X46	1961	12.75	0.500	43.1
31	SMLS	X46	1961	12.75	0.500	57.4
32	SMLS	B	1949	16.0	0.250	46.2
33	SMLS	B	1949	16.0	0.312	47.9
34	SMLS	B	1947	16.0	0.313	43.4
35	SMLS	X52	Unk.	18.0	0.332	55.2
36	SMLS	X42	1944	24.0	0.281	43.5
37	SMLS	X42	1944	24.0	0.281	45.8
38	SMLS	X42	1944	24.0	0.281	47.7

Replicas were mounted on glass slides for transportation and imaging in the laboratory. In both cases, the microstructures were viewed using a standard laboratory metallograph at magnifications from 100x to 500x based on the observed grain size.

Quantitative analyses of the microstructures were performed using both counting and comparison methods to assess the grain size of the ferrite. These methods were adapted from ASTM standards, and the details of the methods are provided elsewhere [23]. The grain sizes are presented here in terms of the mean linear intercept  $\bar{L}$ , which is related to the standard ASTM grain size  $G$  by

$$\bar{L} = 320 \cdot 2^{-\frac{G}{2}} \text{ [\mu m]} \tag{7}$$

### Implementing the Model

The predicted yield strengths  $\sigma_y$  can be calculated from Eq. 6 using the literature-based coefficients found in Table 1. However, measured values for dislocation density  $\rho$  were unavailable for the current set of pipes and are likely to be unavailable in any practical field applications. The approach used for the current pipe set was to equate the contribution of dislocation strengthening in each pipe  $\sigma_{dis}$  to the difference between the 0.5% yield strength from tensile testing ( $\sigma_{TT}$ ) and the sum of  $\sigma_0 + \sigma_{SS} + \sigma_{GS}$  from Eq. (6):

$$\sigma_{dis} = M \cdot \alpha \cdot G \cdot b \cdot \rho^{0.5} = \sigma_{TT} - [\sigma_0 + \sigma_{SS} + \sigma_{GS}] \tag{8}$$

Rearranging Eq. (8) to solve for  $\rho$  yields:

$$\rho = \left[ \frac{\sigma_{TT} - (\sigma_0 + \sum C_i \% A_i + k \cdot d^{-0.5})}{M \cdot \alpha \cdot G b} \right]^2 \tag{9}$$

An analysis of the distribution of  $\rho$  values obtained from Eq. (9) indicates that  $\sqrt{\rho}$  is normally distributed. A statistical description of  $\sqrt{\rho}$  and  $\sigma_{dis}$  is shown in Table 3 for the analysis using NDT

**Table 3.** Statistical analysis of dislocation densities determined from NDT results using Eq. (8). Percentages indicate probabilities based on the normal distribution of  $\rho^{0.5}$ .

	$\rho^{0.5}, \text{ cm}^{-1}$ ( $\times 10^5$ )	$\sigma_{dis},$ ksi
Average	1.53	17.1
St. Dev.	0.473	5.3
Max.	2.49	27.8
Min.	0.732	8.2
95%	2.31	25.8
90%	2.13	23.9
10%	0.923	10.3
5%	0.751	8.4

data. The average and standard deviation of  $\sqrt{\rho}$  correspond to an average and standard deviation for  $\rho$  of  $2.34 \times 10^{10} \text{ cm}^{-2}$  and  $0.223 \times 10^{10} \text{ cm}^{-2}$ , respectively, with corresponding values of 17.1 ksi and 5.3 ksi for  $\sigma_{dis}$ . Based on these, the corresponding 95% / 5% probability values are 25.8 and 8.4 ksi. Applying the average value for the dislocation density to all the pipes in the set yields a constant value of 17.1 ksi for  $\sigma_{dis}$  and introduces a potential error that is likely to be less than  $\pm 6.8$  ksi for 80% of the results and  $\pm 8.7$  ksi for 90% of the results. Similar results (17.0 ksi for  $\sigma_{dis}$ ) were obtained from the analysis using input values for grain size and chemistry from laboratory destructive testing (DT) rather than field NDT.

**Table 4.** Reported dislocation densities measured in polygonal and quasi-polygonal ferrite grains in low carbon steels.

Reference	%C	Dislocation Density, cm <sup>-2</sup>	Comments
6	0.08	6.9x10 <sup>9</sup>	X52 line pipe
13	0.03	(3.9±1.97)x10 <sup>10</sup>	
15	0.06	5.8 - 12.4x10 <sup>10</sup> (air cooled)	TMCP
24	0.05	(1.8±0.2)x10 <sup>10</sup>	
25	0.06	2.0 - 3.0x10 <sup>10</sup>	60% acicular ferrite
26	0.10	1.9x10 <sup>10</sup>	Measured in ferrite phase
27	0.11	16.4x10 <sup>10</sup> (as-rolled)	Polygonal and quasi-polygonal ferrite
28	0.00	13.3x10 <sup>10</sup> (as-rolled)	Pure Fe

The model in Eq. (6) can therefore be restated using the constant approximations for  $\sigma_{dis}$  of 17.0 ksi for DT results or 17.1 ksi for NDT results. These approximations are based on Eq. (4), the values for  $M\alpha$ ,  $G$ , and  $b$  from Table 3, and the underlying estimates of  $2.30 \times 10^{10} \text{ cm}^{-2}$  or  $2.34 \times 10^{10} \text{ cm}^{-2}$  for the dislocation density,  $\rho$ . As a result, Eq. (6) becomes:

$$\sigma_Y = \sigma_0 + \sum(C_i \cdot \%A_i) + k \cdot d^{-0.5} + \begin{pmatrix} 17.0 \text{ ksi for DT} \\ 17.1 \text{ ksi for NDT} \end{pmatrix} \quad (10)$$

From a practical perspective, the values of  $2.30 \times 10^{10} \text{ cm}^{-2}$  versus  $2.34 \times 10^{10} \text{ cm}^{-2}$  are equivalent, with the difference representing less than 1% of  $\sigma_{dis}$ , or an average of less than 0.6% of the total  $\sigma_Y$ . They are presented here to illustrate the consistency of the model despite the different data sources. These estimated dislocation densities are generally consistent with prior reports [6,13,15,24-28]. While the modern literature regarding dislocation density in steel ferrite grains appears to be largely focussed on high strength steels, with most of the easily accessible, relevant data originating from measurements in steels with less than 0.1% C, this should not affect the relevance to higher C steels since the actual C content in the ferrite is limited to approximately 0.02%. A few relevant reports of dislocation densities measured in polygonal and quasi-polygonal ferrite are tabulated in Table 4.

## Results and Discussion

### Comparison to Tensile Testing

Figure 1 compares  $\sigma_{TT}$  to  $\sigma_Y$  calculated from Eq. (10) using the values in Table 1 and  $\rho$  of  $2.30 \times 10^{10} \text{ cm}^{-2}$  or  $2.34 \times 10^{10} \text{ cm}^{-2}$  for the DT and NDT results, respectively. No additional optimization of the model was performed as part of the analysis. The  $\sigma_{TT}$  determined from tensile testing is plotted versus the calculated (model) values for  $\sigma_Y$ . In the plots, the unity line is shown in grey, the linear fit by the dashed red line, and the 95% prediction interval by the dotted red lines. The analysis shows similar results from both the DT and NDT data, with slopes near 1.05, intercepts near -3 ksi, and  $R^2$  values near 0.75. These suggest a linear correlation between the model and the measured results, with a model mean near unity and moderate scatter. The average 95% prediction intervals over the range from 30 ksi to 90 ksi are: DT of  $\pm 12.1$  ksi and NDT of  $\pm 11.8$  ksi. On average,

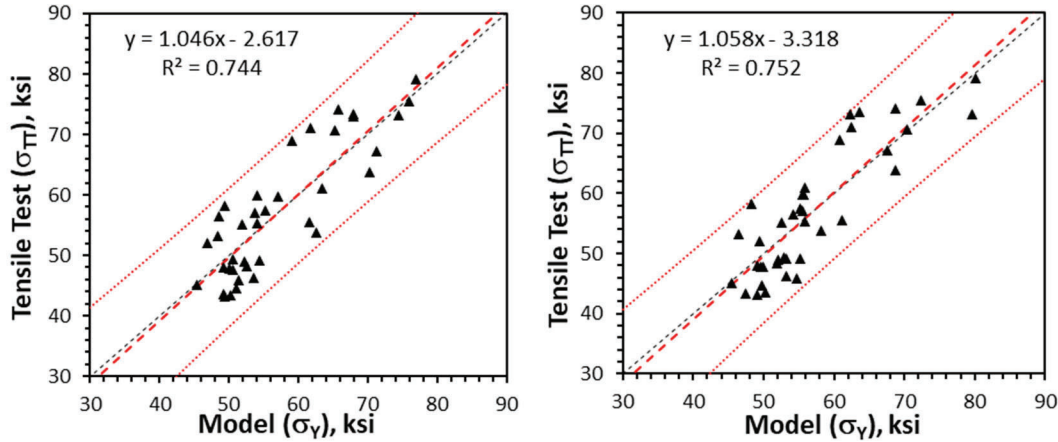


Figure 1.  $\sigma_{TT}$  from tensile testing versus  $\sigma_Y$  from Eq. (6) using  $d$  and  $\%A_i$  from (l) DT, and (r) NDT. Average dislocation densities were estimated to be  $2.30 \times 10^{10} \text{ cm}^{-2}$  and  $2.34 \times 10^{10} \text{ cm}^{-2}$  for DT and NDT results, respectively.

Table 5. Contributions of the different strengthening mechanisms to the results shown in Fig. 1.

	DT, ksi				NDT, ksi			
	$\sigma_0$	$\sigma_{SS}$	$\sigma_{GS}$	$\sigma_{dis}$	$\sigma_0$	$\sigma_{SS}$	$\sigma_{GS}$	$\sigma_{dis}$
Avg	7.8	5.9	26.5	17.0	7.8	5.9	26.2	17.1
Max	7.8	9.7	43.5	17.0	7.8	9.5	46.8	17.1
Min	7.8	2.2	17.6	17.0	7.8	2.1	17.3	17.1

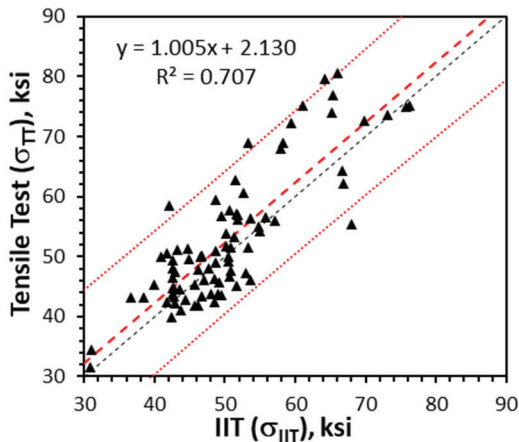


Figure 2.  $\sigma_{TT}$  from tensile testing versus  $\sigma_{IIT}$  from 83 pipes. The black, dashed line shows the linear fit and the red, dotted lines show the 95% prediction intervals (average  $\pm 12.2$  ksi).

the  $\sigma_0$ ,  $\sigma_{SS}$ ,  $\sigma_{GS}$ , and  $\sigma_{dis}$  terms contribute 14%, 10%, 46%, and 30% of the predicted yield strength, Table 5.

### Comparison to Instrumented Indentation Testing

For comparison, Figure 2 shows a similar representation of IIT validation data using 83 line pipes [29]. The unity plot shows the 0.5% EUL from tensile testing ( $\sigma_{TT}$ ) versus the yield strength estimated from IIT ( $\sigma_{IIT}$ ). The LLSR fit is comparable to the model fits shown in Figure 1, with a slope near 1.0, an  $R^2$  of 0.71, and a 95% prediction interval with an average value of  $\pm 12.2$  ksi over the range shown. To facilitate the comparison between the model predictions and the IIT results, Figure 3 shows unity plots for the subset of 30 pipes included in both the model data (Figure 1) and the IIT validation data

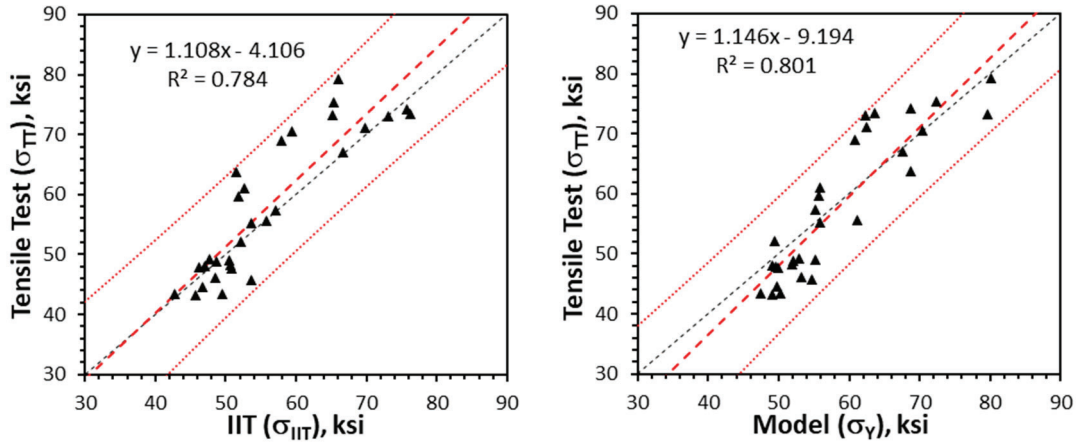


Figure 3. (l) Subset of the IIT results in Figure 2 for the 30 pipes included in the current pipe set, and (r) model predictions using NDT data for the same 30 pipes. The 95% prediction intervals are (l)  $\pm 12.5$  ksi, and (r)  $\pm 12.0$  ksi.

(Figure 2). The left-hand plot shows  $\sigma_{TT}$  versus the measured  $\sigma_{IIT}$ , and the right-hand plot shows the corresponding plot for  $\sigma_{TT}$  versus the model-predicted  $\sigma_Y$ . The results again suggest that the model provides comparable performance to IIT measurements. The 95% confidence intervals are comparable, 12.5 ksi for the IIT and 12.0 ksi for the model, and the MAPE values are 6.8 for the IIT and 8.2 for the model. Note again that the pipe set used in this study includes only ferrite-pearlite microstructures and does not consider more complex microstructures that can result from accelerated cooling rates.

### Unconstrained LLSR Fit

As a point of interest, Eq. (10) can be fit to the test data using linear least squared regression (LLSR) fitting to optimize the values of  $\sigma_0$ ,  $\sigma_{dis}$ ,  $C_i$  and  $k$  for the current pipe set. In that case, Eq. (10) becomes:

$$\sigma_Y = \sigma'_0 + C_{Mn} \cdot \%Mn + C_{Cu} \cdot \%Cu + C_{Si} \cdot \%Si + C_{Cr} \cdot \%Cr + k \cdot d^{-0.5} \quad (11)$$

where the constant  $\sigma_0$  and  $\sigma_{dis}$  terms have been combined into a single constant,  $\sigma'_0$ . This approach provides the best opportunity for the model to accurately reflect the tensile test results; however, unconstrained fitting of the coefficients undermines the basis of the historical model and ties the validity of the fitted model to the makeup of the current pipe set.

Figure 4 shows  $\sigma_{TT}$  plotted against the model described by Eq. (11) and Table 6. The plots show improved model performance, with increased  $R^2$  values of  $\approx 0.89$  and decreased 95% prediction intervals of  $\pm 7.6$  ksi and  $\pm 7.8$  ksi for the DT and NDT results, respectively. On average, the  $\sigma'_0$  ( $= \sigma_0 + \sigma_{dis}$ ),  $\sigma_{SS}$ , and  $\sigma_{CS}$ , and terms contribute 38% - 39%, 31% - 33%, and 26% - 30% of the predicted yield strength, respectively (Table 7). Note that the average contribution of  $\sigma'_0$ ,  $\approx 22$  ksi, is generally consistent with the sum of the  $\sigma_0$  and  $\sigma_{dis}$  terms from Table 5.

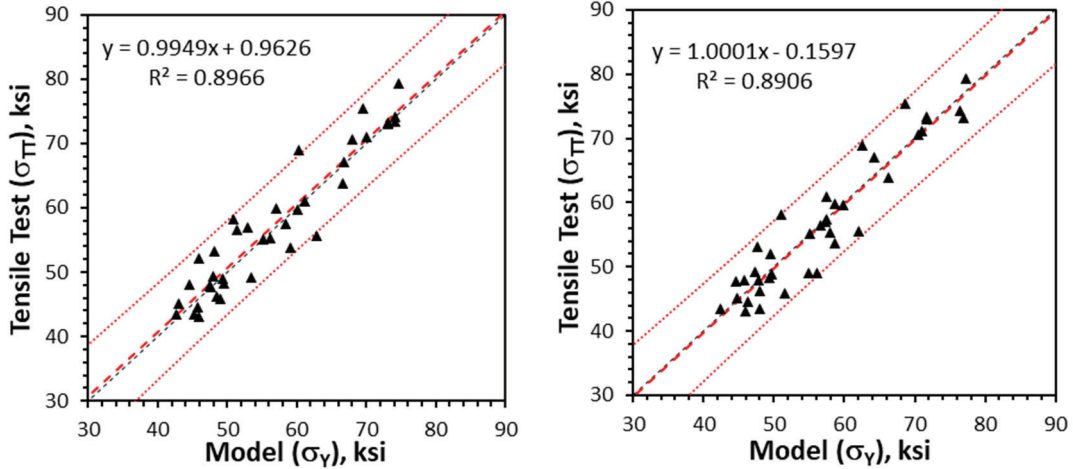


Figure 4.  $\sigma_{TT}$  from tensile testing versus  $\sigma_{\gamma}$  from Eq. (11) using  $d$  and  $\%A_i$  from (l) DT, and (r) NDT.

Table 6. Values of the model parameters obtained from LLSR fitting Eq. (11). Published values ('Literature') are shown for reference.

Parameter	DT	NDT	Literature	Units
$\sigma_0'$	149.4	153.5	N/A	MPa
$k$	9.8	11.5	17.4	MPa· $\sqrt{\text{mm}}$
$M\alpha$	N/A	N/A	0.38	-
$G$	N/A	N/A	$81.6 \times 10^3$	MPa
$b$	N/A	N/A	0.249	nm
$C_{Si}$	182.1	158.7	85	MPa
$C_{Cu}$	283.1	295.0	39	MPa
$C_{Mn}$	107.8	91.0	32	MPa
$C_{Cr}$	0.00	0.00	-30	MPa

Table 7. Contribution of the different strengthening mechanisms to the results shown in Figure 4.

	DT, ksi			
	$\sigma_0'$	$\sigma_{SS}$	$\sigma_{GS}$	$\sigma_{dis}$
Avg	21.7	20.0	14.9	N/A
Max	21.7	35.0	24.4	N/A
Min	21.7	8.0	9.9	N/A

	NDT, ksi			
	$\sigma_0'$	$\sigma_{SS}$	$\sigma_{GS}$	$\sigma_{dis}$
Avg	22.3	17.6	17.3	N/A
Max	22.3	31.4	30.8	N/A
Min	22.3	6.6	11.4	N/A

## Summary and Conclusions

This investigation illustrates the use of an historical strength model for steel to estimate yield strength from grain size and composition in line pipe steels. Results from a set of 38 non-microalloyed line pipes with hot-rolled, ferrite-pearlite microstructures (not quenched and tempered) suggest that the model performance for estimating yield strength is comparable to instrumented indentation testing when using only literature values for coefficients. The only fitting performed to optimize the model was to estimate the average dislocation density for the set of pipes. The use of literature-based coefficients decreases the risk of model dependence on the makeup of the pipe set used for 'calibration'. For comparison, the model was fit to the existing pipe set by using LLSR to optimize the coefficients. That fitted model exhibits improved performance; however, the approach is not recommended due to the unknown effect of the fitting process on the general applicability of the model (i.e., to steels that are not well represented by the pipe set used in the fitting). The results suggest that this model may be a useful tool to confirm strength testing by in-ditch NDT, provide strength estimates where in-ditch NDT is not practical, or replace some fraction of NDT strength testing altogether.

## References

- [1] B Amend, M Gould, P Veloo, O Oneal, R Gonzalez, N Switzner (2021) "In Situ Metallography Applications in the Pipeline Industry," *Materials Evaluation* 79 (8), 790-796.
- [2] M Gould, B Amend, P Veloo, O Oneal, R Gonzalez, N Switzner, (2021) "The role of in-situ metallography in pipeline integrity management," in *Proceedings of The Pipeline Pigging and Integrity Management Conference, PPIM 2021*, Paper #51.
- [3] P Martin, N Switzner, J Anderson, J Stuckner, O Lopez-Oneal, S Curiel, and P Veloo (2024) "A Machine Learning Model to Automate Quantitative Evaluation of Line Pipe Microstructures," in *Proceedings of The Pipeline Pigging and Integrity Management Conference, PPIM 2024*, Paper #274.
- [4] N Switzner, P Veloo, M Rosenfeld, T Rovella, J Gibbs, (2020) "An approach to establishing manufacturing process and vintage of line pipe using in-situ nondestructive examination and historical manufacturing data," in *Proceedings of The International Pipeline Conference, IPC-2020*, Paper #84461.
- [5] N Switzner, S Thorsson, J Kornuta, P Veloo, P Martin, T Rovella, M Rosenfeld (2020) "Influence of line pipe steel microstructure on NDE yield strength predictive capabilities," in *Proceedings of The Pipeline Pigging and Integrity Management Conference, PPIM 2021*.
- [6] O Lavigne, A Kotousov, and V Luzin (2017) "Microstructural, Mechanical, Texture and Residual Stress Characterizations of X52 Pipeline Steel," *Metals*, 7, 306.
- [7] N Kamikawa, K Sato, G Miyamoto, M Murayama, N Sekido, K Tsuzaki, and T Furuhashi (2015) "Stress-strain behavior of ferrite and bainite with nano-precipitation in low carbon steels," *Acta Mat.*, 83, 383.
- [8] G Liu, "Designing with Carbon-, Low-, and Medium-alloy Steels," in *Handbook of Mechanical Alloy Design*, GE Totten, L Xie, and K Funatani, Eds. (Taylor & Francis Inc., Marcel Dekker Inc., New York, NY, USA, 2004) pp. 73-89.
- [9] FB Pickering, *Physical Metallurgy and the Design of Steels*, (Applied Science Publishers, London, UK, 1978) p. 63.

- 
- [10] EOB Hall (1951) "The deformation and aging of mild steel: I. The effects of strain rate, temperature, and aging upon the properties of mild steel," *Proc. of the Phys. Soc., Section B*, 64, 747-753.
- [11] NJ Petch (1953) "The cleavage strength of polycrystals," *J. Iron and Steel Inst.*, 174, 25-28.
- [12] MA Altuna, A Iza-Mendia, and I Gutierrez, (2008) "Precipitation strengthening produced by the formation in ferrite of Nb carbides," in *Proceedings of the 3<sup>rd</sup> International Conference on Thermomechanical Processing of Steels* (Padova, Italia, 10-12 September 2008).
- [13] JR Yang, HKDH Bhadeshia (1990) "The dislocation density of acicular ferrite in steel welds," *Weld. Res. Suppl.*, 69, 305s-307s.
- [14] GI Taylor (1934) "The Mechanism of Plastic Deformation of Crystals. Part I.—Theoretical.," *Proc. R. Soc. Lond., Ser. A145*, 362-388.
- [15] V Carretero Olalla, V Bliznuk, N Sanchez, P Thibaux, LAI Kestens, and R H Petrov (2014) "Analysis of the strengthening mechanisms in pipeline steels as a function of the hot rolling parameters," *Mat. Sci. Eng. A*, 604, 46-56.
- [16] M.F. Ashby (1970) "The Deformation of Plastically Non-Homogeneous Materials," *Phil. Mag.* 21, 399-424.
- [17] A Dinovitzer, S Tiku, A Hassannejadasl, M Ghovanlou, and N Pussegoda (2016) "In The Ditch Non-Destructive Mechanical Property Measurement for Vintage Low Toughness Pipe," Prepared for Pipeline Research Council International (PRCI), Inc., Contract PR-214-123734, PRCI Report No. NDE4-C.
- [18] JY Kim, KW Lee, JS Lee and D Kwon (2006) "Determination of tensile properties by instrumented indentation technique: Representative stress and strain approach," *Surf. and Coat. Tech.*, 201, 4278-4283
- [19] P Martin, E Brady, J Kornuta, S Thorsson, R Nasouri, J Gibbs and P Veloo (2024) "Exploring the Role of Residual Stress in Correlating Yield Strength from Indentation-Based Nondestructive Measurements and Destructive Tensile Testing," in *Proceedings of The International Pipeline Conference, IPC-2024*, Paper #133508.
- [20] M Louie, B Amend, M Liong, M Gould, N Switzner, T Rovella, P Martin, P Veloo (2019) "Nondestructive Testing of Pipeline Materials: Analysis of Chemical Composition from Metal Filings," in *Proceedings of The Pipeline Pigging and Integrity Management Conference, PPIM 2019*.
- [21] N Switzner, M Liong, P Veloo, M Gould, T Rovella (2020) "Nondestructive Testing of Pipeline Materials: Further Evaluation of Portable OES, XRF, LIBS, and Filings to Estimate Chemical Composition," in *Proceedings of The Pipeline Pigging and Integrity Management Conference, PPIM 2020*.
- [22] J Maragh, C Liu, P Martin, N Switzner, J Gibbs, J Kornuta, P Veloo (2022) "Reducing Bias in Chemical Composition Data with Measurements Below the Limit of Detection," in *Proceedings of The Pipeline Pigging and Integrity Management Conference, PPIM 2022*, Paper #20.
- [23] LP Martin, NT Switzner, O Oneal, S Curiel, J Anderson, and P Veloo (2022) "Quantitative Evaluation of Microstructure to Support Verification of Material Properties in Line-Pipe Steels," in *Proceedings of The International Pipeline Conference, IPC-2022*, Paper #87063.
- [24] EV Morales, RA Silva, IS Bott, and S Paciornik (2013) "Strengthening mechanisms in a pipeline microalloyed steel with a complex microstructure," *Mat. Sci. Eng., A* 585, 253-260.
- [25] A Mandal, B Syed, K Bhandari, B Bhattacharya, A Deb, SB Singh, and D Chakrabarti (2019) "Cold-bending of linepipe steel plate to pipe, detrimental or beneficial?," *Mat. Sci. Eng., A*, 746, 58-72.
- [26] N Kamikawa, K Sato, G Miyamoto, M Murayama (2015) "Stress-strain behavior of ferrite and bainite with nano-precipitation in low carbon steels," *Acta Mat.*, 83, 383-396.
- [27] K Horiuchi, T Ogawa, Z Wang, and Y Adachi (2021) "Three-dimensional analysis of ferrite grains recrystallized in low-carbon steel during annealing," *Materials*, 14, 4154.

- [28] S Sugiyama, T Ogawa, L He, Z Wang, Y Adachi (2021) “Quantitative analysis of the recovery process in pure iron using X-ray diffraction line profile analysis,” *Materials*, 14, 895.
- [29] M Scales, J Anderson, JA Kornuta, N Switzner, R Gonzalez and P Veloo (2022) “Accurate Estimation of Yield Strength and Ultimate Tensile Strength through Instrumented Indentation Testing and Chemical Composition Testing,” *Materials*, 15, 832.